Augmented Models of High-Frequency Transformers for SMPS

Augmented models of High-Frequency Transformers for SMPS

I. A. Maio, P. Savi, I. S. Stievano, F. G. Canavero

Dipartimento di Elettronica, Politecnico di Torino
Corso Duca degli Abruzzi 24, 10129, Torino, Italy
igor.stievano@polito.it

***Abstract*—The modeling of high-frequency transformers via augmented equivalent circuits is addressed. The augmented models are composed of a low-frequency equivalent and a supplemental element modeled via real rational fitting. They offer both high accuracy levels and a physical meaning that helps the interpretation of simulation results. Parasitics effects between the windings and between the windings and the carrying board can be also included. The use of an augmented model for the simulation of a dc-dc converter is demonstrated.**

I. Introduction

The modeling of high-frequency transformers is a primary issue in the simulation of Switching Mode Power Suppliers (SMPSs) for EMC predictions. The noise properties of SMPS, in fact, are strongly influenced by the parasitic parameters of their transformers. The required models should be able to reproduce the transformer behavior in the conducted emission range, *i.e.,* from some tens of KHz to 30 MHz, or, possibly, up to higher frequencies. Besides, in order to account for the transformer effects on the common mode noise, the models should include both the coupling between the transformer windings and the coupling to the circuit reference. Modeling approaches based on the physics of the transformer are hardly effective for this modeling problem, that is best addressed via identification methods applied to measured responses. As an example, this approach is exploited in [1], [2] and, recently, in [3], that tackle the modeling of high-voltage and high-power transformers via measurements and model identification.

Unfortunately, models obtained via identification methods have no physical link with the properties of the modeled devices and do not help the interpretation of the simulation results. In contrast, models based on equivalent circuits of the transformer can offer great insight in the operation of the circuits where the modeled device is included. Of course, the prices for this insight are difficulties in estimating the model parameters, that are nonlinearly related to the device responses, and a limited accuracy due to the biasing of the model structure.

In order to exploit both the advantages of identification and equivalent circuit based models, this paper addresses the modeling of an high-frequency transformer via augmented equivalent circuit models. These models are defined by a suitable equivalent circuit of the coupled inductors augmented by an n-port element obtained via identification methods. The parameters of the equivalent circuit are estimated by fitting the low-frequency part of the measured responses. Then a supplemental admittance matrix is defined by the difference $\mathbf{Y}_{sup} = \mathbf{Y} - \mathbf{Y}_{ec}$, where $\mathbf{Y}_{ec}$ is the admittance matrix of the equivalent circuit. This supplemental matrix collects all the parasitic effects not included in the equivalent circuit and is modeled by real rational functions.

In this paper, an augmented model is developed for an example transformer and is applied to the analysis of the noise properties of the SMPS of Fig. 7. Possible common mode effects are addressed by treating the transformer as a four-port element.

II. Experimental Characterization

The measurement of the transformer responses is based on the test fixture shown in Fig. 1. The Device Under Modeling (DUM) is a sample of the two-windings high-frequency transformer Kaschke SNK-12-3. The test fixture is composed of a copper board – that mimics the reference plane where the device is mounted in actual applications – and of four SMA connectors defining four electromagnetic ports between each transformer terminal and the copper plane. The four-port characterization allows to include all the parasitics between the windings and between the windings and the reference plane.

Fig. 1. Test fixture for the measurement technique proposed in this paper. Top panel: device; bottom panel: measurement ports.

In this work, the DUM is characterized in the band 10kHz–50MHz, including both the functional and the out-of-band behavior of the device. The measurement procedure described in [3] is used. It is based on the measurement of a set of one-port responses by either an impedance analyzer or a network analyzer. Four independent one-port responses are obtained for each port by using four different load conditions for the

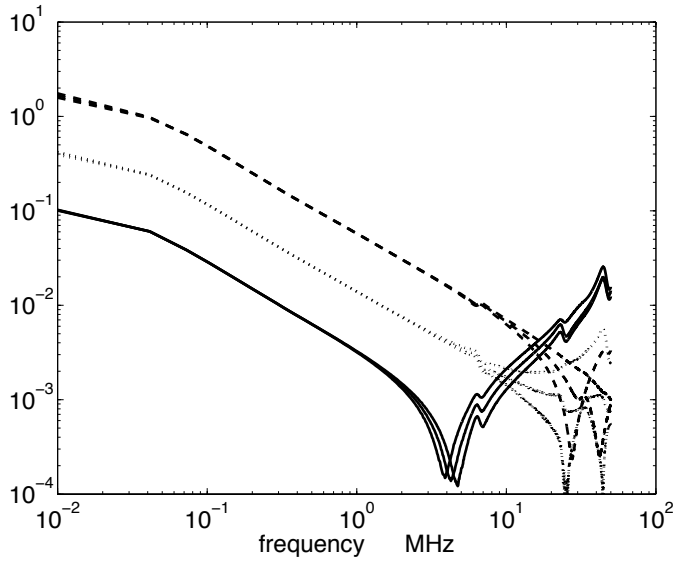

Fig. 2. Measured magnitude in Ω^{-1} of the short circuit admittance matrix elements vs. frequency in MHz for the device under test. Solid lines: Y_{11}, Y_{12}, Y_{22}; dashed lines: Y_{33}, Y_{34}, Y_{44}; dotted lines: Y_{13}, Y_{14}, Y_{24}.

remaining three ports. In order to facilitate the modeling, the port responses are turned into admittances and the result of the characterization phase is the matrix of single port admittances $\bar{Y}^n_{mm}$ defined as:

- $\bar{Y}^m_{mm}$ admittance at port m with all other ports shorted
- $\bar{Y}^n_{mm}$, $n \neq m$ admittance at port m with port n open and all other ports shorted

It is worth noticing that responses with shorted and open ports improve the accuracy of the derived models in describing the device behavior for actual load conditions (*e.g.,* see [2] and Sec. IV).

In order to keep control over the passivity of the developed model, it is expedient to apply the model identification procedure to a standard network characteristic matrix. For this reason, the matrix of the measured admittances is converted into the admittance matrix $\mathbf{Y}$. The elements of $\mathbf{Y}$ are computed as:

$$Y_{mn} = \begin{cases} \bar{Y}^n_{mm} & \text{for } n = m \\ \pm\sqrt{(\bar{Y}^m_{mm} - \bar{Y}^n_{mm})\bar{Y}^n_{nn}} & \text{for } n \neq m \end{cases} \quad (1)$$

In the above relation, off-diagonal terms have uncertain sign, because the use of one-port responses does not yield information of the sign of the transmission responses. For the DUM, however, the correct signs are decided by the orientation of the windings.

Since the device under modeling is reciprocal, $\mathbf{Y}$ is expected to be symmetric and the ten measured admittances $\bar{Y}^n_{mm}$, $m = 1, \ldots, 4$, $n = m, \ldots, 4$ are sufficient to compute the elements of $\mathbf{Y}$. On the other hand, the use of all $\bar{Y}^n_{mm}$ functions allows to check the symmetry of the estimated $\mathbf{Y}$ matrix, verifying the accuracy of the overall process. The ten elements of the admittance matrix estimated for the DUM are shown in Fig. 2.

III. Augmented Models

In this Section, the development of augmented models for the device characterized by the admittances of Fig. 2 is discussed. In the low-frequency part of Fig. 2, only three curves can be distinguished and the estimated admittance matrix has the following structure

$$\mathbf{Y} \approx \begin{bmatrix} +Y_A & -Y_A & -Y_M & +Y_M \\ -Y_A & +Y_A & +Y_M & -Y_M \\ -Y_M & +Y_M & +Y_B & -Y_B \\ +Y_M & -Y_M & -Y_B & +Y_B \end{bmatrix} \quad (2)$$

where $Y_A \approx Y_{11} \approx -Y_{12} \approx Y_{22}$, $Y_B \approx Y_{33} \approx -Y_{34} \approx Y_{44}$ and $Y_M \approx -Y_{13} \approx Y_{14} \approx -Y_{24}$. This is the admittance matrix of a two-port element, whose port A is defined by the terminals no. 2 and no. 1 of the DUM and whose port B is defined by terminals no. 3 and no. 4, according to the schematic of Fig. 3. The frequency range where this structure of the responses

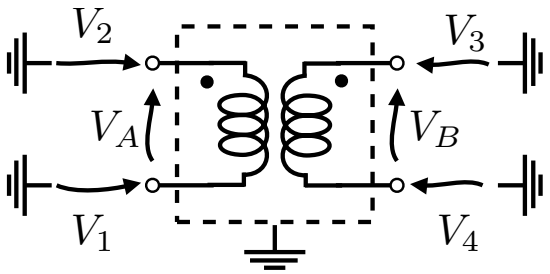

Fig. 3. Labels and reference directions used for the terminals of the device under modeling.

holds extends up to about 2 MHz. It can be concluded that the DUM behaves as a pure two-port element up to about 2 MHz and that only above that frequency the currents coupled to the reference copper plane becomes significant, leading to a four-port behavior. This property suggest to extract a low-frequency equivalent circuit of the DUM by fitting its (two-port) responses up to 2 MHz. It is also clear that the low-frequency part of the DUM is dominated by the inductive behavior of the transformer windings. The main components of the equivalent circuit are, therefore, two coupled inductors.

In order to estimate the parameters of this equivalent circuit, it is expedient to fit its response to the impedance response of the DUM, so that a linear relation between the circuit parameters and the responses holds. The two-port impedances of the DUM are obtained by inverting the 2-port admittance matrix

$$\mathbf{Y}_2 \approx \begin{bmatrix} Y_A & Y_M \\ Y_M & Y_B \end{bmatrix} \quad (3)$$

and are shown in Fig. 4. Of course the curves of such Figure are a correct representation of the DUM impedances up to 2 MHz only. These response are characterized by a pure low-frequency inductive behavior followed by a parallel resonance. This first resonance is likely to be due to the self capacitance of the primary winding, and this suggest the low-frequency equivalent circuit of Fig. 5.

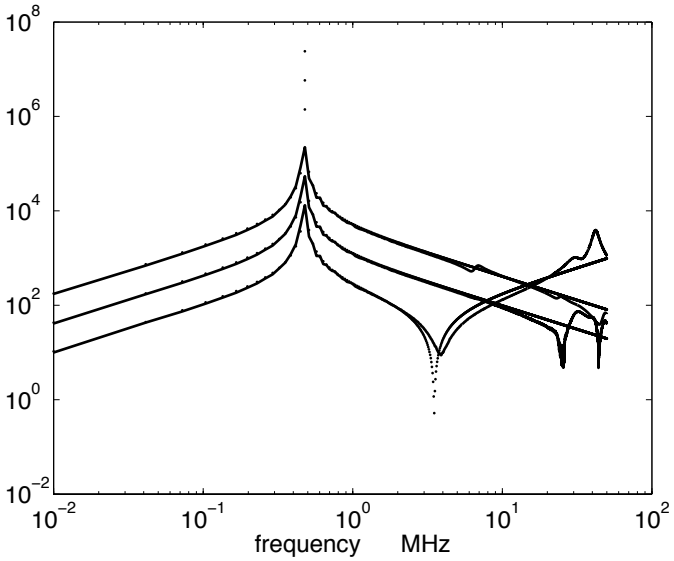

Fig. 4. Magnitude (Ω) of the low frequency entries of the DUM impedance matrix vs. frequency (solid lines) and magnitudes of the impedances of the equivalent circuit of Fig. 5 (dots). From top to bottom, the curves correspond to Z_A, Z_M and Z_B, respectively. The curves represent the actual responses up to 2 MHz only.

The parameters of the coupled inductors (L_1, L_2 and M) and of the resistors (R_1 and R_2) are estimated from the low-frequency part of the curves of Fig. 4, *i.e.,* up to 100 kHz, via linear least square fitting. The capacitance of the circuit is estimated from the frequency of the parallel resonance and from L_1 as $C = 1/(L_1\omega_o^2)$, where ω_o is the angular frequency of the resonance. When the response of the equivalent circuit estimated in this way is plotted, the dotted curves of Fig. 4 are obtained. The agreement of the equivalent circuit and measured response is good up to the parallel resonance.

The equivalent circuit of Fig. 5 is expected to take into account the main operational behavior of the DUM. In order to fit the admittance matrix of the DUM, the circuit is augmented by adding a supplemental four-port element. The admittance matrix of the supplemental element is defined by

$$\mathbf{Y}_{sup} = \mathbf{Y} - \mathbf{Y}_{ec} \tag{4}$$

where $\mathbf{Y}_{ec}$ is the admittance matrix of the equivalent circuit estimated above.

The element defined by $\mathbf{Y}_{sup}$ can be modeled by real rational fitting. Different real rational models can be obtained by using different fitting bandwidths and different number of poles. Each model is defined by a common pole set and is implemented for transient simulations as an equivalent circuit or as a state space realization. We carry out the fitting of $\mathbf{Y}_{sup}$ by means of the IDEM (Identification of linear Electric Models [4]) modeling tool, that is based on the vector fitting method and features an advanced utility to enforce the passivity of estimated models. Details on the modeling process can be found in [5]. Different models can be used to satisfy different accuracy and modeling domain specifications with the minimal possible complexity.

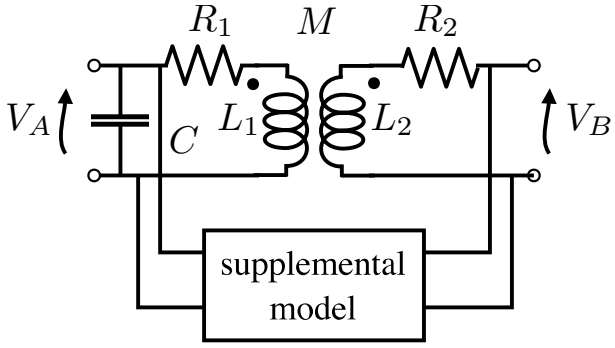

Fig. 5. Schematic of the augmented model developed in Sec. III. The coupled inductors and the capacitor define the low-frequency equivalent circuit that is augmented by the supplemental four-terminals element obtained via real rational identification.

An example of the admittance responses of the supplemental element and of their rational fitting up to 2 MHz is shown in Fig. 6. This example is aimed at obtaining an augmented model for the analysis of the converter of Fig. 7. Since the waveforms of this converter do not show significant noise component above the 2MHz boundary, a simple two-port model is developed.

The admittance curves of the supplemental element maintain a residual low-frequency inductive component that is one order of magnitude smaller than the original one shown in Fig. 2. The rational model of Fig. 6 is defined by eight poles and features a maximum relative error on the order of 3×10^{-3} in the fitting range. This is also the maximum error between the measured admittance responses and the admittance responses of the resulting augmented model up to 2 MHz.

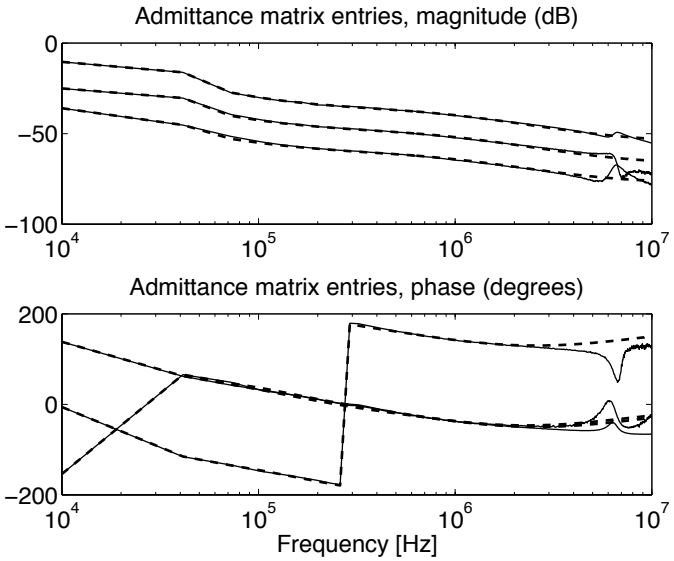

Fig. 6. Magnitude (top panel, dB/Ω^{-1}) and Phase (bottom panel, degree) vs. frequency for the Y_{supB}, Y_{supM}, Y_{supA} (from top to bottom) admittance functions. Solid lines: admittance data estimated from measurement; dashed lines: responses of the rational model estimated by IDEM (fitting up to 2 MHz by 8 poles)

IV. Simulation Example

The example transformer of Fig. 1 is designed for SMPS circuits applications. In this Section, the augmented model proposed is applied to the simulation of the fly-back dc-dc converter Fig. 7. The four-terminal element of this Figure represents the modeled transformer and the aim of the simulation is to reproduce and explain the transient waveforms of the converter, that are responsible for its noise emissions.

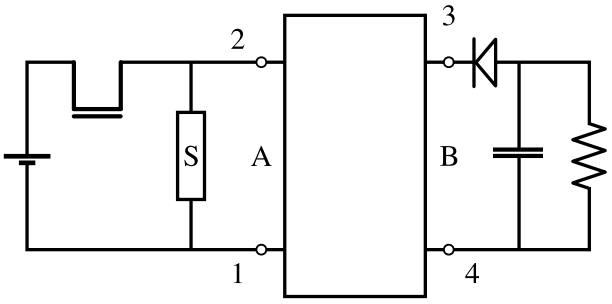

Fig. 7. Block diagram of a Fly-back dc-dc converter using the high-frequency transformer modeled in this paper. The converter uses a MOSFET switching device and a snubber circuit for noise suppression (the 2-terminal element with label S).

The simulation is carried out by SPICE and the script of the simulation includes the augmented model of the transformer, a behavioral model of the MOSFET switch, an RC snubber with series diode and no layout parasitics. The switching events of the MOSFET are tuned to match the waveforms measured on the actual converter. The waveform computed by means of the SPICE script for the voltage across port A of the transformer and the actual measured waveforms are shown in Fig. 8. Two simulated waveforms are included: the dashed line curve is obtained by representing the transformer by means of its equivalent circuit only, whereas the solid line curve is obtained by using the complete augmented model. Though the prediction obtained from the equivalent circuit is less accurate than those of the complete model, it reproduces well the qualitative behavior of the waveform. The equivalent circuit, therefore can help the interpretation of the waveform.

In Fig. 8, the rectangular pulses correspond to the on time intervals of the MOSFET switch, whereas the rest of the waveform correspond to the off time intervals. In the off time interval there is a flat part of the response (where the diode of port B is the on state and the current of the primary winding is transferred to the output capacitor) and a relaxation oscillation part. The relaxation oscillation occurs when the voltage of the secondary winding becomes smaller than the capacitor voltage and the diode turns to off state. In this condition, the relaxation oscillation that are observed are caused by the resonance of the inductance L_1 and of the capacitor C (*e.g.,* see the frequency of the parallel resonance of Fig. 4). In contrast, the resonance between the capacitor and the leakage inductance of the coupled inductors, that should occur during the on state of the diode, is not observed, because it is effectively dumped by the snubber circuit. If the snubber is disconnected, then the expected resonance appears.

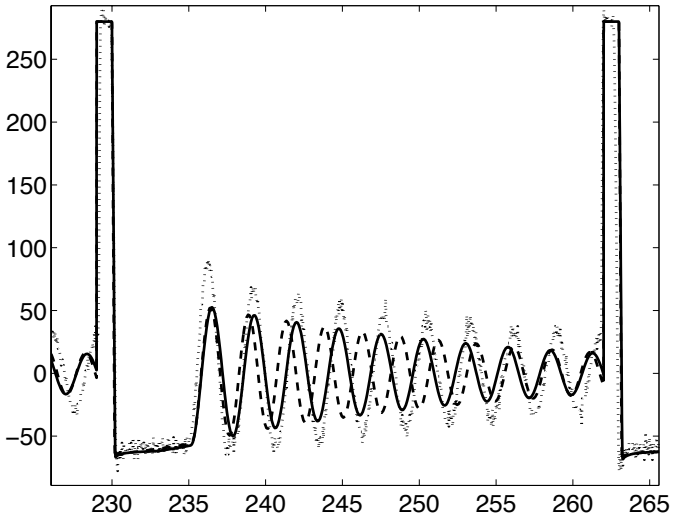

Fig. 8. Voltage (V) at port A of the transformer of the fly-back converter of Fig. 7 vs. time (μs). Solid line: SPICE simulation based on the augmented transformer model; dashed line: SPICE simulation based on the equivalent circuit of the transformer; Dotted line: measurement.

V. Conclusions

The modeling of high-frequency transformers via augmented equivalent circuits is addressed. The procedure is illustrated on an example device. The equivalent circuit part of the model is derived by the low-frequency response of the DUM and the supplemental part of the model is estimated via real rational fitting. The model obtained in this way is accurate as well as efficient and physically meaningful. For the application shown, the equivalent circuit part of the model helps the complete interpretation of the circuit waveform. Of course the proposed approach holds for both two-port and four-port problems allowing for common mode couplings.

References

[1] S.-K. Chung, "Transient characterisctis of high-voltage flyback trasformer operating in discountinous conduction mode", *IEE Proc.-Electr. Power Appl.* Vol. 151, No. 5, pp. 628-634, September 2004.

[2] B. Gustavsen, "Wide band modeling of power trasformer", *IEEE Trans. Power Delivery*, Vol. 19, No. 1, pp. 414-422, January 2004.

[3] I.A. Maio, F.G. Canavero, R. Franchino, D. Leonard, P. Savi, "Experimental Characterization and Modeling of High-Frequency Transformers for SMPS , *Proc. Of Embedded Systems and Electromagnetic Compatibility, 2emc*, Rouen (France), October 18-19, 2007

[4] see the IDEM Section on *www.emc.polito.it*

[5] F.G. Canavero, S. Grivet-Talocia, I.A. Maio, I.S. Stievano, "Linear and Nonlinear Macromodels for System-Level Signal Integrity and EMC Assessment", *IEICE Trans. on Communications - Special Issue on EMC*, Vol. E88-B, No. 8, August 2005.